

Luminescent gold–silver complexes derived from neutral bis(perfluoroaryl)diphosphine gold(i) precursors†

Cite this: *Dalton Trans.*, 2013, **42**, 4267

R. Vilma Bojan,^a Rafal Czerwieniec,^{*b} Antonio Laguna,^c Tania Lasanta,^a José M. López-de-Luzuriaga,^{*a} Miguel Monge,^a M. Elena Olmos^a and Harmut Yersin^{*b}

Complex $[\text{Au}\{4\text{-C}_6\text{F}_4(4\text{-C}_6\text{BrF}_4)\}(\text{tht})]$ reacts with diphosphines (L–L) such as bis(diphenylphosphino)methane (dppm) or 1,2-bis(diphenylphosphino)benzene (dppb) in a 2 : 1 molar ratio in dichloromethane, leading to neutral products of stoichiometry $[(\text{Au}\{4\text{-C}_6\text{F}_4(4\text{-C}_6\text{BrF}_4)\})_2(\mu\text{-L-L})]$ (L–L = dppm (**1**), dppb (**2**)). In the crystal structure of complex **2** short Au...Au interactions of 2.9367(5) and 2.9521(5) Å appear. This complex displays an orange emission, which is assigned to arise from a charge transfer transition from a metal centered Au–Au orbital to an orbital located at the diphosphine ligand. Addition of silver trifluoroacetate to these complexes in a 1 : 1 or a 2 : 1 molar ratio generates polymeric heterometallic gold–silver compounds of stoichiometry $[\text{Ag}_2\text{Au}_2\{4\text{-C}_6\text{F}_4(4\text{-C}_6\text{BrF}_4)\}_2(\text{CF}_3\text{CO}_2)_2(\mu\text{-L-L})_n]$ (L–L = dppm (**3**), dppb (**4**)), which confirms the capability of the neutral $[(\text{Au}\{4\text{-C}_6\text{F}_4(4\text{-C}_6\text{BrF}_4)\})_2(\mu\text{-diphosphine})]$ units to act as electron density donors when treated with a Lewis acid substrate. These heterometallic derivatives show blue emissions indicating large HOMO–LUMO band gaps, due to the stabilization that the gold-based HOMO orbitals suffer when the electron withdrawing silver trifluoroacetate fragments interact with them.

Received 20th July 2012,
Accepted 18th December 2012

DOI: 10.1039/c2dt32973e

www.rsc.org/dalton

Introduction

Aurophilic Au(i)···Au(i) interactions have traditionally been the most studied nonbonding contacts between closed-shell metal ions.¹ However, over the past few years, complexes with metallophilic interactions between gold(i) centres and other closed-shell metal atoms (Au···M) have attracted great interest due to their theoretical interest,² photophysical properties³ or potential applications.⁴ In this sense, the presence of a heavy gold atom (Au) in these complexes enhances the spin orbit coupling of the systems, which in turn facilitates the access to triplet excited states *via* intersystem crossing. In addition, the possibilities of electronic transitions are numerous, thus the lowest excited states may be of metal-centred (MC), ligand-to-metal

charge transfer (LMCT), metal-to-ligand charge transfer (MLCT), metal-to-metal charge transfer (MMCT), ligand-to-ligand charge transfer (LLCT) and intraligand charge transfer (IL) types.⁵ Nevertheless, the use of phosphines as ligands allows the interaction of metal pπ and phosphine π-acceptor orbitals generating low-energy empty π orbitals in the ligands, which are available as acceptor orbitals for MLCT transitions, although a mixed MLCT/MC excited state cannot either be excluded.

Additionally in these systems, a strategy that permits the tuning of the emission is to incorporate electron donating or accepting groups, which modify the relative energy of the frontier orbitals in the coordination sphere of the gold centres. In that sense, our group has contributed a number of examples in which heteronuclear complexes are formed by Lewis acid–base reactions between basic gold complexes and metallic acid salts. Usually, the stability of these complexes is enhanced by an appreciable ionic component because the metallic fragments are of opposite charge. In those examples, the main ionic character of the interaction makes the excited states to arise from MMCT transitions and, therefore, the direct comparison of the energies of the transitions with those observed for the precursor gold complexes is not possible.

Also, a recent strategy consists of the synthesis of heteronuclear complexes starting from neutral precursors. In this

^aDepartamento de Química, Universidad de La Rioja, Centro de Investigación en Síntesis Química (CISQ), Complejo Científico-Tecnológico, 26004-Logroño, Spain.
E-mail: josemaria.lopez@unirioja.es

^bInstitut für Physikalische und Theoretische Chemie, Universität Regensburg, Universitätstr. 31, D-93040 Regensburg, Germany.

E-mail: rafal.czerwieniec@chemie.uni-regensburg.de,
harmut.yersin@chemie.uni-regensburg.de

^cDepartamento de Química Inorgánica, Instituto de Ciencia de Materiales de Aragón, Universidad de Zaragoza-CSIC, 50009-Zaragoza, Spain

†CCDC 891443–891445. For crystallographic data in CIF or other electronic format see DOI: 10.1039/c2dt32973e

way, the metal–metal interactions are formed by weaker van der Waals forces and the charge transfer component that dominated the excited state in the former is diminished.

On the other hand, as it is well known, the neutral derivatives $[\text{Au}(\text{C}_6\text{X}_5)(\text{tht})]$ (X = halogen, tht = tetrahydrothiophene) are important starting materials for the synthesis of gold(I) complexes through displacement reactions of the weakly coordinated tht ligand by other neutral or anionic ligands, resulting in the formation of mononuclear $[\text{Au}(\text{C}_6\text{X}_5)\text{L}]$ or $[\text{Au}(\text{C}_6\text{X}_5)\text{X}']^-$ (L , X' = monodentate ligands) or polynuclear compounds $[\{\text{Au}(\text{C}_6\text{X}_5)\}_n\text{L}]_n$ or $[\{\text{Au}(\text{C}_6\text{X}_5)\}_n\text{X}']_n^-$ (L , X' = polydentate ligands) that often display aurophilic interactions.⁶ With these precedents, we wondered if the neutral diaryl derivative $[\text{Au}\{4\text{-C}_6\text{F}_4(4\text{-C}_6\text{BrF}_4)\}(\text{tht})]$ could react with diphosphines, in order to obtain basic gold(I) compounds where the presence of intramolecular interactions is favoured by the bidentate ligand. The choice of this diaryl precursor is based on the experience acquired by our group in reactions with bis(perhalophenyl)aurate(I) derivatives and acid metallic salts, in which the basicity of the gold precursor is strongly influenced by the type of aryl groups.^{4b,c,7,8} In addition, phosphines are well known to stabilize electron-rich transition metals in low oxidation states due to the important π back bonding.

As Lewis acid we have chosen the dinuclear silver(I) trifluoroacetate, whose acid capability is very high as we have shown in previous papers.^{7–9}

Taking into account all above, we studied the behaviour of the new diaryldiphosphine gold(I) derivatives $[\text{Au}\{4\text{-C}_6\text{F}_4(4\text{-C}_6\text{BrF}_4)\}(\text{L})]$ (L = dppm, dppb) as electron density donors by treating them with the Lewis acid silver(I) trifluoroacetate. The crystal structures of the resulting complexes have been determined by X-ray diffraction methods, and their optical properties have been experimentally and theoretically studied in order to rationalize the results.

Results and discussion

Synthesis and characterization

Compounds $[\{\text{Au}\{4\text{-C}_6\text{F}_4(4\text{-C}_6\text{BrF}_4)\}\}_2(\mu\text{-L-L})]$ (L-L = bis(diphenylphosphino)methane (dppm) (1) or 1,2-bis(diphenylphosphino)benzene (dppb) (2)) were obtained by reactions of $[\text{Au}\{4\text{-C}_6\text{F}_4(4\text{-C}_6\text{BrF}_4)\}(\text{tht})]$ and the selected diphosphines in a 2:1 molar ratio, using dichloromethane as a solvent. As expected, the reactions occur with displacement of the weakly bound tetrahydrothiophene as a free ligand and in almost quantitative yields (see eqn (1)).

Complexes 1 and 2 are isolated as white solids, stable to air and moisture at room temperature. They are soluble in dichloromethane, tetrahydrofuran, acetone and diethyl ether, and insoluble in *n*-hexane.

Analytical and spectroscopic data of complexes 1 and 2 agree well with the stoichiometries (see the Experimental section). Their IR spectra show, among others, absorptions at ~ 1630 , ~ 1600 , ~ 1570 , ~ 1100 and ~ 855 cm^{-1} arising from the presence of the $4\text{-C}_6\text{F}_4(4\text{-C}_6\text{BrF}_4)$ group bonded to gold(I), and

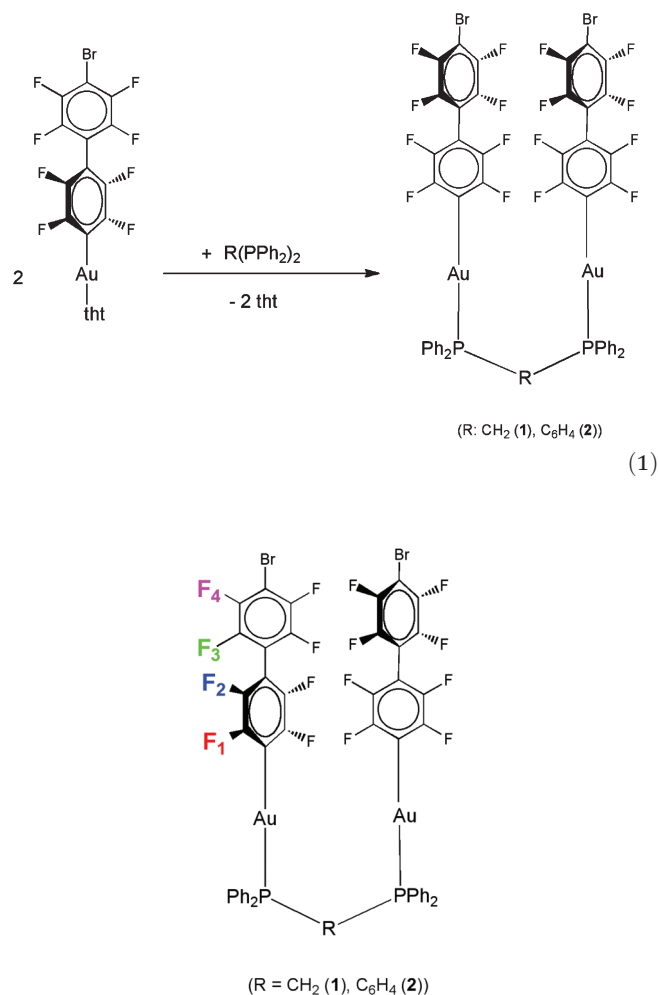


Fig. 1 Identification of the four inequivalent fluorine atoms in compounds 1 and 2.

at $548\text{--}461$ cm^{-1} due to the bidentate diphosphine ligands. Mass spectra (MALDI-TOF(-)) show signals corresponding to $[\text{Au}\{4\text{-C}_6\text{F}_4(4\text{-C}_6\text{BrF}_4)\}_2]^-$ at m/z = 949 (100%).

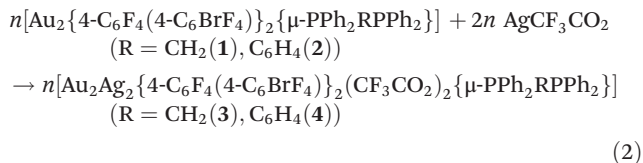
The ^1H NMR spectra of complexes 1 and 2 recorded in CDCl_3 show signals at 7.80–7.28 ppm (1) and 7.62–7.26 ppm (2), corresponding to the aromatic hydrogen atoms. Besides, in the spectrum of 1 a triplet at 3.65 ppm is present ($^2J_{(\text{H-P})} = 9.2$ Hz) due to the methylenic hydrogens, which are coupled with both equivalent phosphorus atoms of the dppm ligand.

The ^{19}F NMR spectra of complexes 1 and 2 show four multiplets corresponding to the four inequivalent fluorine atoms in the $4\text{-C}_6\text{F}_4(4\text{-C}_6\text{BrF}_4)$ ligand at -116.5 , -133.9 , -137.1 and -140.5 ppm (1) or -114.7 , -133.5 , -137.2 and -141.0 ppm (2) for $\text{F}_1\text{--F}_4$, respectively (see Fig. 1). The positions for the signals observed in the ^{19}F NMR spectrum for complex 1 are similar to those described for the starting material $[\text{Au}\{4\text{-C}_6\text{F}_4(4\text{-C}_6\text{BrF}_4)\}(\text{tht})]$.¹⁰ However, the signal for F_1 in complex 2 is shifted to down field.

The $^{31}\text{P}\{^1\text{H}\}$ NMR spectra of these complexes display a singlet at 32.3 (1) and 34.1 ppm (2), which confirms the

equivalence of the phosphorus atoms in the molecule and their coordination to the gold centres.

Treatment of $[(\text{Au}\{4\text{-C}_6\text{F}_4(4\text{-C}_6\text{BrF}_4)\})_2(\mu\text{-L-L})]$ (L-L = bis(diphenylphosphino)methane (dppm) (1) or 1,2-bis(diphenylphosphino)benzene (dppb) (2)) with silver trifluoroacetate in dichloromethane, in a 1 : 1 or a 1 : 2 molar ratio, leads to the formation of heterometallic gold silver compounds $[\text{Ag}_2\text{Au}_2\{4\text{-C}_6\text{F}_4(4\text{-C}_6\text{BrF}_4)\}_2(\text{CF}_3\text{CO}_2)_2(\mu\text{-L-L})]_n$ (L-L = dppm (3), dppb (4)) (see eqn (2)).



Reactions of these precursors with the silver salt in different molar ratios lead in all cases to a mixture of complexes 3 or 4 and the metal complex added in excess.

Complexes 3 and 4 are isolated as pale yellow solids, stable to air and moisture at room temperature. They are soluble in dichloromethane, tetrahydrofuran, acetone and diethyl ether, and insoluble in *n*-hexane.

Analytical and spectroscopic data of these complexes agree with the proposed stoichiometries (see the Experimental section). Their IR spectra show, among others, absorptions at 1571, ~1100 and 856 cm^{-1} arising from the presence of the $\{4\text{-C}_6\text{F}_4(4\text{-C}_6\text{BrF}_4)\}$ group bonded to gold(I), at 547–459 cm^{-1} corresponding to the phosphine ligands, and at ~1645 and ~1180 cm^{-1} due to C–O and C–F stretching modes, which confirms the presence of trifluoroacetate anions in the molecule.

The ^1H NMR spectra in CDCl_3 of complexes 3 and 4 show the signals corresponding to the methylenic (3) and aromatic hydrogen atoms (3, 4) at similar shifts to those described for compounds 1 and 2, respectively.

The ^{19}F NMR spectra of complexes 3 and 4 show four multiplets corresponding to the four inequivalent fluorine atoms in the aromatic ligand $4\text{-C}_6\text{F}_4(4\text{-C}_6\text{BrF}_4)$ at –115.6, –133.7, –137.0 and –140.0 ppm (3) or –114.2, –133.4, –137.2 and –140.7 ppm (4) for F₁–F₄, respectively. In addition, the CF₃ group of the trifluoroacetate ligands appears at –73.1 (3) and –73.3 ppm (4).

Finally, the $^{31}\text{P}\{^1\text{H}\}$ NMR spectra of these complexes display a singlet at 32.4 (3) and 33.9 ppm (4), which confirms the equivalence of the phosphorus atoms in the molecule and their coordination to the gold centres.

The resemblance between the spectroscopic data of complexes 3 and 4 with those of their precursor complexes would be in agreement with the loss of the intermetallic interactions in solution.

X-ray structural determination of derivatives 2, 3 and 4

Single crystals suitable for X ray diffraction studies of complex 2 were obtained by slow diffusion of *n*-hexane into a saturated solution of the complex in dichloromethane. The crystal structure for 2 shows two dinuclear molecules of $[\text{Au}_2\{4\text{-C}_6\text{F}_4\text{-}$

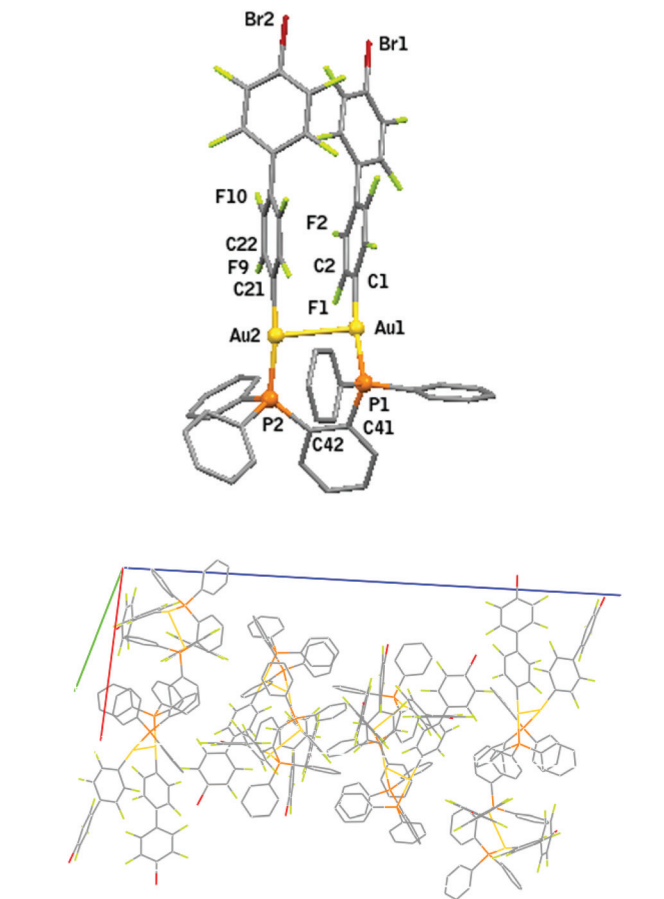


Fig. 2 Crystal structure of one molecule (up) and packing of molecules in the crystal (bottom) for compound 2. Hydrogen atoms are omitted for clarity.

$(4\text{-C}_6\text{BrF}_4)_2\{\mu\text{-1,2-C}_6\text{H}_4(\text{PPh}_2)_2\}]$ in the asymmetric unit, where the diphosphine ligand acts as a bridge between the two gold centres. A perspective view of the $[\text{Au}_2\{4\text{-C}_6\text{F}_4(4\text{-C}_6\text{BrF}_4)\}_2\{\mu\text{-1,2-C}_6\text{H}_4(\text{PPh}_2)_2\}]$ molecule and the packing in the crystal of 2 are shown in Fig. 2.

In this complex the Au–Au distances are 2.9367(5) and 2.9521(5) Å, which are considered Au...Au intramolecular interactions (see Table 2). The shortest intermolecular Au–Au distance is 8.323 Å, which excludes any considerable metal–metal intermolecular interaction. Thus, the $[\text{Au}_2\{4\text{-C}_6\text{F}_4(4\text{-C}_6\text{BrF}_4)\}_2\{\mu\text{-1,2-C}_6\text{H}_4(\text{PPh}_2)_2\}]$ molecules in the crystal of 2 can be regarded as isolated molecules in a rigid crystalline environment.

Each gold atom is coordinated to the *ipso* carbon of the bis(perhalophenyl) ligand, with normal Au–C and Au–P bond distances between 2.045(10) and 2.063(9) Å, and between 2.272(2) and 2.295(3) Å, respectively, the longer ones being similar to those found in related complexes of the type $[\text{Au}_2(\text{aryl})_2(\mu\text{-L-L})]$.¹¹

The environment of the gold centres shows a deviation from the linearity, with C–Au–P angles in the range 173.8(3)–169.3(3)°, probably due to the presence of aurophilic intramolecular interactions aided by the rigidity generated by the

Table 1 Data collection and structure refinement details for 1–3

Compound	2	3·0.5C ₆ H ₁₄ ·H ₂ O	4·0.5CH ₂ Cl ₂
Chemical formula	C ₅₄ H ₂₄ Au ₂ Br ₂ F ₁₆ P ₂	C ₅₃ H ₂₂ Ag ₂ Au ₂ Br ₂ F ₂₂ O ₄ P ₂ ·0.5C ₆ H ₁₄ ·H ₂ O	C ₅₈ H ₂₄ Ag ₂ Au ₂ Br ₂ F ₂₂ O ₄ P ₂ ·0.5CH ₂ Cl ₂
Crystal habit	Colourless prism	Colourless prism	Colourless plate
Crystal size/mm	0.3 × 0.28 × 0.2	0.25 × 0.25 × 0.2	0.35 × 0.3 × 0.15
Crystal system	Monoclinic	Triclinic	Triclinic
Space group	<i>P</i> 2 ₁ / <i>n</i>	<i>P</i> 1	<i>P</i> 1
<i>a</i> /Å	15.3232(3)	13.0125(6)	12.1335(3)
<i>b</i> /Å	17.5150(5)	14.8392(5)	15.0322(6)
<i>c</i> /Å	37.5226(9)	17.5999(7)	18.1077(7)
<i>α</i> /°	90	91.369(2)	102.664(1)
<i>β</i> /°	99.901(1)	110.783(2)	91.933(2)
<i>γ</i> /°	90	92.024(2)	107.338(2)
<i>V</i> /Å ³	9920.5(4)	3172.9(2)	3058.51(19)
<i>Z</i>	8	2	2
<i>D_c</i> /g cm ⁻³	2.132	2.126	2.255
<i>M</i>	1592.43	2031.22	2076.67
<i>F</i> (000)	6000	1910	1950
<i>T</i> /°C	−150	−173	−150
2θ _{max} /°	56	56	56
μ(Mo-Kα)/mm ⁻¹	7.683	6.637	6.929
No. refl. measured	124 465	47 997	49 615
No. unique refl.	23 182	14 985	14 674
<i>R</i> _{int}	0.0701	0.0627	0.0549
<i>R</i> [<i>F</i> > 2σ(<i>F</i>)] ^a	0.0637	0.0576	0.0675
w <i>R</i> [<i>F</i> ² , all refl] ^b	0.1259	0.1558	0.2387
No. of refl. used	23 182	14 985	14 674
No. of parameters	1369	798	856
No. of restraints	332	33	190
<i>S</i> ^c	1.197	1.043	1.125
Max. residual electron density/e Å ⁻³	4.599	4.815	3.430

^a $R(F) = \sum ||F_o| - |F_c|| / \sum |F_o|$. ^b $wR(F^2) = [\sum \{w(F_o^2 - F_c^2)^2\} / \sum \{w(F_o^2)^2\}]^{0.5}$; $w^{-1} = \sigma^2(F_o^2) + (aP)^2 + bP$, where $P = [F_o^2 + 2F_c^2]/3$ and a and b are constants adjusted by the program. ^c $S = [\sum \{w(F_o^2 - F_c^2)^2\} / (n - p)]^{0.5}$, where n is the number of data and p the number of parameters.

Table 2 Selected bond lengths [Å] and angles [°] for complex 2

Au(1)–C(1)	2.058(9)	Au(3)–C(101)	2.063(9)
Au(2)–C(21)	2.045(10)	Au(4)–C(121)	2.053(10)
Au(1)–P(1)	2.277(3)	Au(3)–P(3)	2.272(2)
Au(2)–P(2)	2.295(3)	Au(4)–P(4)	2.278(3)
Au(1)–Au(2)	2.9367(5)	Au(3)–Au(4)	2.9521(5)
C(1)–Au(1)–P(1)	173.8(3)	C(101)–Au(3)–P(3)	173.5(3)
C(21)–Au(2)–P(2)	169.8(3)	C(121)–Au(4)–P(4)	169.3(3)

1,2-C₆H₄(PPh₂)₂ ligand. The aromatic rings in the 4-C₆F₄–(4-C₆BrF₄) ligands display dihedral angles of 52.12(29)° and 58.80(30)°, lower than the value described for the free ligand: 60.2(1)°. ¹²

Single crystals suitable for X-ray diffraction studies of complexes 3·0.5C₆H₁₄·H₂O and 4·0.5CH₂Cl₂ were obtained by slow diffusion of *n*-hexane into a saturated solution of the complexes in dichloromethane, both of them crystallizing with the solvent. Crystal structures of 3·0.5C₆H₁₄·H₂O and 4·0.5CH₂Cl₂ are formed by the repetition of alternating dinuclear [Au₂{4-C₆F₄(4-C₆BrF₄)₂(μ-L-L)}] (L-L = dppm, dppb) and [Ag₂(CF₃CO₂)₂] units, which are connected by short unsupported Au...Ag contacts, generating polymeric chains (see Fig. 3 and 4).

These Au...Ag interactions, of 2.8377(7) and 2.7984(8) Å in 3·0.5C₆H₁₄·H₂O, and 2.9106(10) and 2.8532(9) Å in 4·0.5CH₂Cl₂, are in general shorter than those described for

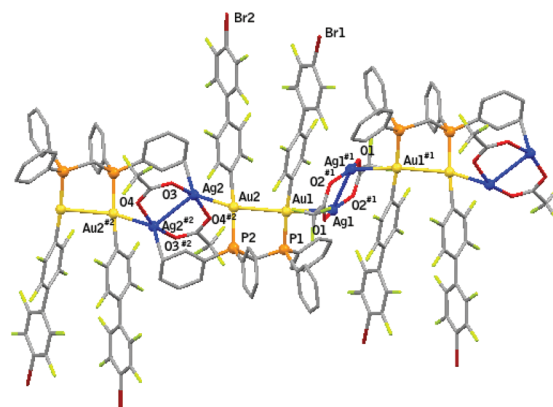


Fig. 3 Expansion of the crystal structure for compound 3. Hydrogen atoms are omitted for clarity. Colour code: gold: yellow; silver: blue; phosphorous: orange; carbon: grey; oxygen: red; fluorine: light green; bromine: dark red.

other polymeric Au/Ag species, such as [AuAgR(CF₃CO₂)(tbt)]_n (R = C₆F₅, C₆Cl₅), [AuAg₂(C₆Cl₂F₃)(CF₃CO₂)₂(tbt)]_n, ⁸ [AuAg₄(mes)(RCO₂)₄(tbt)_x]_n ($x = 1$, R = CF₃, CF₂CF₃; $x = 3$, R = CF₂CF₃; mes = mesityl, 2,4,6-C₆Me₃H₂), {[AuAg₄(mes)(CF₃CO₂)₄(tbt)(H₂O)]·H₂O·CH₂Cl₂]_n, ^{7a} (NBu₄)₂[AuAg₄(C₆Cl₂F₃)₂(CF₃CO₂)₅]_n ^{7b} or [AuAg₃(C₆F₅)(CF₃CO₂)₃(CH₂PPh₃)]_n, ⁹ where the Au–Ag distances lie in the range of 2.8135(5)–3.1347(7) Å (average value of 2.9054 Å) (see Table 3 and 4).

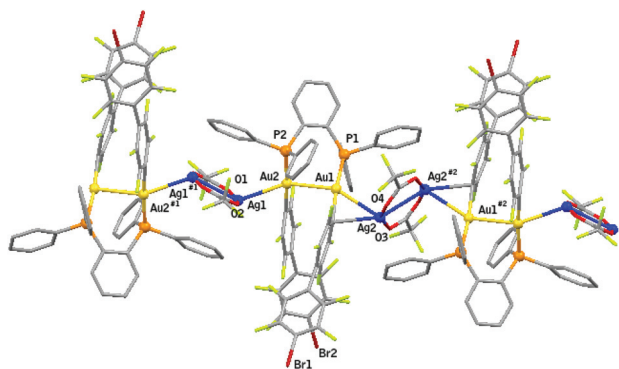


Fig. 4 Expansion of the crystal structure for compound **4**. Hydrogen atoms are omitted for clarity. Colour code: gold: yellow; silver: blue; phosphorous: orange; carbon: grey; oxygen: red; fluorine: light green; bromine: dark red.

Table 3 Selected bond lengths [Å] and angles [°] for complex **3**·0.5C₆H₁₄·H₂O

Au(1)–C(1)	2.052(8)	Ag(1)–O(1)	2.184(8)
Au(2)–C(21)	2.047(9)	Ag(1)–O(2)#1	2.181(7)
Au(1)–P(1)	2.287(2)	Ag(2)–O(3)	2.204(8)
Au(2)–P(2)	2.275(2)	Ag(2)–O(4)#2	2.233(9)
Au(1)–Au(2)	2.9830(5)	Ag(2)–C(75)#2	2.666(12)
Au(1)–Ag(1)	2.8377(7)	Ag(1)–Ag(1)#1	2.8214(14)
Au(2)–Ag(2)	2.7984(8)	Ag(2)–Ag(2)#2	2.8860(16)
C(1)–Au(1)–P(1)	174.8(2)	O(2)#1–Ag(1)–O(1)	157.7(2)
C(21)–Au(2)–P(2)	173.9(3)	O(3)–Ag(2)–O(4)#2	160.3(3)
Ag(1)–Au(1)–Au(2)	149.85(2)	Ag(1)#1–Ag(1)–Au(1)	123.30(4)
Ag(2)–Au(2)–Au(1)	139.90(2)	Au(2)–Ag(2)–Ag(2)#2	122.49(4)

Symmetry transformations used to generate equivalent atoms: #1 $-x + 1, -y + 2, -z + 1$ #2 $-x + 2, -y + 1, -z + 1$.

Table 4 Selected bond lengths [Å] and angles [°] for complex **4**·0.5CH₂Cl₂

Au(1)–C(1)	2.079(13)	Ag(1)–Ag(1)#1	2.8605(16)
Au(2)–C(21)	2.044(9)	Ag(2)–Ag(2)#2	2.9293(19)
Au(1)–P(1)	2.268(3)	Ag(1)–O(2)	2.202(9)
Au(2)–P(2)	2.285(2)	Ag(1)–O(1)	2.207(10)
Au(1)–Ag(2)	2.9106(10)	Ag(2)–O(3)	2.213(12)
Au(2)–Ag(1)	2.8532(9)	Ag(2)–O(4)	2.226(12)
Au(1)–Au(2)	2.9884(5)	Ag(2)–C(1)	2.698(12)
C(1)–Au(1)–P(1)	173.0(3)	O(2)–Ag(1)–O(1)	163.6(3)
C(21)–Au(2)–P(2)	175.6(3)	O(3)–Ag(2)–O(4)	157.0(4)
Ag(2)–Au(1)–Au(2)	149.66(3)	Au(2)–Ag(1)–Ag(1)#1	133.47(5)
Ag(1)–Au(2)–Au(1)	145.08(3)	Au(1)–Ag(2)–Ag(2)#2	114.05(5)

Symmetry transformations used to generate equivalent atoms: #1 $-x + 1, -y + 1, -z + 1$ #2 $-x + 1, -y, -z$.

In addition to these metal–metal contacts, there are Ag...Ag intramolecular interactions within the silver trifluoroacetate dimers of 2.8214(14) and 2.8860(16) Å in **3**·0.5C₆H₁₄·H₂O, and 2.8605(16) and 2.9293(19) Å in **4**·0.5CH₂Cl₂, obviously favoured by the presence of bridging ligands. Finally, also the gold centres of each dinuclear unit maintain an intermetallic contact of 2.9830(5) Å in **3**·0.5C₆H₁₄·H₂O and 2.9884(5) Å in **4**·0.5CH₂Cl₂. It is worth noting that the Au–Au distances are of the same order in both structures, about 0.04 Å longer than in complex **2**. Therefore, this shortening seems to be a consequence of the incorporation of the [Ag₂(CF₃CO₂)₂] units.

The gold atoms are linearly coordinated to the C_{ipso} of the perhalobiphenyl ligand and to one of the phosphorus of the diphosphine, with normal Au–C (2.044(9)–2.079(13) Å) and Au–P distances (2.268(3)–2.287(2) Å). The aromatic rings in the 4-C₆F₄(4-C₆BrF₄) ligand form dihedral angles between 54.52(15) and 73.90(51)°.

Regarding the silver atoms, it is worth mentioning the presence of a rather unusual Ag...C contact of 2.666(12) Å between one of the silver atoms of each unit and the *meta* carbon of a phenyl group of the diphosphine in the crystal structure of **3**·0.5C₆H₁₄·H₂O. Similarly, one of the silver atoms of each [Ag₂(CF₃CO₂)₂] interacts with one *ipso* carbon of the perhalobiphenyl ligand, with a Ag–C distance of 2.698(12) Å in the case of complex **4**·0.5CH₂Cl₂.

Photophysical properties

The absorption spectra of the precursor gold complexes **1** and **2** in dichloromethane solutions ($\approx 10^{-6}$ mol L⁻¹) display similar features with strong absorptions starting at 225 nm with tails extending to 325 nm. Thus, both show intense maxima at 233 ($\epsilon = 11 \times 10^4$ (1), 9×10^3 mol⁻¹ L cm⁻¹ (2)) and 254 nm ($\epsilon = 13 \times 10^4$ (1), 9.4×10^3 mol⁻¹ L cm⁻¹ (2)). These bands can arise from transitions located in the bis(perhalophenyl) ligand, probably between π – π^* orbitals, and from $\sigma \rightarrow a_\pi$ transitions associated with coordinated phosphines. In fact, the perhalophenyl precursor gold complex [Au{4-C₆F₄(4-C₆BrF₄)}(tht)] displays one absorption at 259 nm, which is red shifted from the corresponding free perhalophenyl (248 nm) and, on the other hand, free phosphines display bands assigned to $l \rightarrow a_\pi$ transitions at higher wavelengths.¹³ Additionally, for both complexes a broadening can be observed in the less energetic region that can be related to the presence of intramolecular gold–gold interactions.

In the case of the heterometallic gold–silver complexes **3** and **4**, the absorption spectra display almost identical features. Thus, complex **3** shows bands at 234 ($\epsilon = 7 \times 10^3$ mol⁻¹ L cm⁻¹) and 254 nm ($\epsilon = 8.3 \times 10^3$ mol⁻¹ L cm⁻¹) and complex **4** at 238 ($\epsilon = 8.7 \times 10^3$ mol⁻¹ L cm⁻¹) and 251 nm ($\epsilon = 9 \times 10^3$ mol⁻¹ L cm⁻¹), respectively. Consequently, we assign these bands to similar origins to that in the precursors. In addition, both show weak non-well resolved bands at 295 nm ($\epsilon = 2.6 \times 10^3$ mol⁻¹ L cm⁻¹ (3)) and 310 nm ($\epsilon = 1.5 \times 10^3$ mol⁻¹ L cm⁻¹ (4)). These bands are not present in the spectra of the phosphines or perhalophenyl ligands. Therefore, we can tentatively assign them to the presence of intermetallic interactions (Au...Au or Au...Ag) (see Fig. 5).

Both Au(i) complexes **1** and **2** as well as the hybrid Au–Ag crystals **3**·0.5C₆H₁₄·H₂O and **4**·0.5CH₂Cl₂ are brightly luminescent. The emission spectra together with the excitation profiles recorded for solid samples at room temperature are reproduced in Fig. 6. Emission maxima, quantum yields and decay times are listed in Table 5.

Crystalline samples of the studied Au(i) complexes show intense green (**1**) and orange (**2**) luminescence with high quantum yields ϕ_{PL} of 58 and 14% for **1** and **2**, respectively. They show broad and unstructured emission bands centered

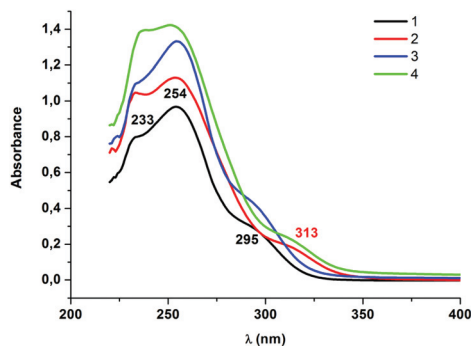


Fig. 5 UV-Vis spectra of complexes **1–4** in dichloromethane.

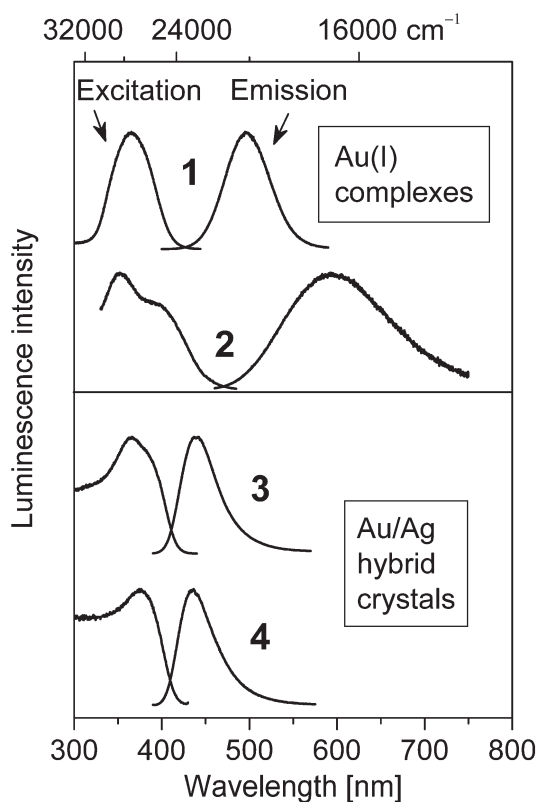


Fig. 6 Room-temperature excitation and luminescence spectra of solid Au(I) complexes **1** and **2** and Au–Ag hybrid crystals **3**·0.5C₆H₁₄·H₂O and **4**·0.5CH₂Cl₂. Emission spectra were recorded upon excitation at $\lambda_{\text{exc}} = 380$ nm. Excitation spectrum of each sample was recorded at a detection wavelength λ_{det} corresponding to the respective emission maximum. Luminescent intensity is in arbitrary units. Energy scale (in cm^{-1}) is given for orientation.

at λ_{max} of 496 (**1**) and 593 nm (**2**), respectively. The emission spectra are considerably red-shifted relative to the lowest-energy absorptions manifested in the excitation spectra (Fig. 6). For instance, for complex **1**, emission maximum ($\lambda_{\text{max}} = 496$ nm) and the lowest absorption band maximum ($\lambda_{\text{abs}} \approx 365$ nm) are separated by *ca.* 7000 cm^{-1} .

On the other hand, the decay times τ_{em} of luminescence determined for **1** and **2** are $\tau_{\text{em}} = 1.5$ and 6.2 μs , respectively. Such high τ_{em} values show that these emissions represent

Table 5 Summary of the photophysical properties of Au(I) complexes **1** and **2** and hybrid Au–Ag compounds **3**·0.5C₆H₁₄·H₂O and **4**·0.5CH₂Cl₂ determined for solid samples at ambient temperature. Respective emission spectra are drawn in Fig. 6. All measurements were carried out under an inert N₂ atmosphere

	RT λ_{em}^a [nm]	Emission decay time τ_{em} [μs]	Photoluminescence quantum yield ϕ_{PL}^d [%]
1	496	1.5 ^b	58
2	593	6.2 ^b	14
3	439	2.5 ^b	24
4	436	0.3 ^b	<3 ^e
		1.0 ^c	

^a Experimental error ± 1 nm. ^b Experimental error ± 0.2 μs . ^c The decay is distinctly non-monoexponential. The measured decay profile could be successfully fitted only by using a biexponential decay function. ^d Experimental error $\pm 3\%$. ^e ϕ_{PL} of this material lies below the resolution threshold of our setup, which is about 3%.

largely forbidden transitions. Therefore, they are assigned as phosphorescence from the lowest excited triplet state T_1 to the ground state S_0 . Intensive $T_1 \rightarrow S_0$ emissions with ϕ_{PL} of tens of percent and radiative decay times of several microseconds are frequently found for organometallic compounds of transition metal ions (mostly 3-rd row, *e.g.* Pt, Ir, Au),¹⁴ in which strong spin–orbit coupling (SOC) induced by the heavy metal atom leads to effective mixing of the triplet and singlet wavefunctions.^{14a,15} In particular, the lowest triplet state can get certain contributions from higher lying singlet states and, as a result, the formally spin-forbidden $T_1 \rightarrow S_0$ transition becomes partly allowed. Compounds with distinctly strong SOC, like Ir-tris(2-phenylpyridine), Ir(ppy), may show ϕ_{PL} values of almost 100% with an emission decay time τ_{em} in the order of 1 microsecond.^{14b,16}

The large difference between the energy of the emissions in complexes **1** and **2** suggests that, in this case, a metal centred Au–Au transition is not likely, since as it is expected, small differences in metal–metal distances in the complexes should not lead to important changes in the energy of the emissions. On the other hand, an intraligand (IL) $\pi\pi^*$ transition located in the diaryl groups or in the phosphine ligand can be excluded because more energetic emissions should be expected. Also metal (gold) to ligand (bis(perfluoroaryl)) charge transfer (MLCT) transitions can also be ruled out, since in such cases similar emissions should be expected for both complexes. What it seems likely is that the photophysical properties of **1** and **2** strongly depend on the bridging diphosphine ligand. However, the exact role of the dppm and dppb ligands is difficult to assess. Among the possibilities, reasonable assumptions are, for example, that the emissions can arise from a metal (gold) to ligand (phosphine) charge transfer (MLCT), or from a ligand (bis(perfluoroaryl)) to ligand (phosphine) charge transfer. Especially in the case of complex **1**, an ILCT associated with the $\sigma \rightarrow a_x$ transition in the phosphine cannot be ruled out, since its emission appears at similar energies than those reported for other gold–diphosphine complexes in which the emissions were assigned to have that origin.¹³

Interestingly, the reaction between the gold complexes **1** and **2** and silver trifluoroacetate with the subsequent formation of heterometallic Au–Ag structures leads to considerable changes in the photophysical behaviour. Both mixed-metal Au–Ag crystals of **3** and **4** display blue luminescence, with $\lambda_{\text{max}} = 439$ and 436 nm, respectively. Interestingly, compound **3** displays a high luminescence quantum yield of 24% while the decay time is determined to be $\tau_{\text{em}} = 2.5$ μs . As in the precursor complexes, they do not show emissive properties in solution and the lifetimes suggest phosphorescent processes (see Table 5). In principle, the origins of the electronic transitions that give rise to the luminescence can be similar to the precursor gold complexes (see above), nevertheless a curious blue shift, which is larger in the case of complex **2**, is observed when silver trifluoroacetate is incorporated into the structure.

Taking into account the molecular structures of complexes **2** and **4**, the Au–Au distance in $[\text{Ag}_2\text{Au}_2\{4\text{-C}_6\text{F}_4(4\text{-C}_6\text{BrF}_4)\}_2(\text{CF}_3\text{CO}_2)_2(\mu\text{-dppb})]_n$ is only 0.04 Å longer than that found for complex **2**. This small variation seems not to be responsible for a blue shift of more than 6500 cm^{-1} . Consequently, the interacting gold centres seem not to be the only responsible for the transitions, although the blue shift suggests the stabilization of the HOMO orbitals, probably due to the electron withdrawing silver trifluoroacetate fragments interacting with them. Therefore, what it seems likely is that the emissions arise from transitions between the electron rich bis(perhalophenyl) groups to empty antibonding orbitals of the phosphines and that the introduction of the electron withdrawing silver trifluoroacetate diminishes the electron density in those ligands through the gold centres, stabilizing the HOMO orbitals and shifting the emissions to higher energies. In order to get more insight into the orbital nature of the emitting state DFT computational studies on models of the complexes were performed (see below).

DFT calculations

In view of the different photophysical properties observed experimentally for the dinuclear diphosphinogold(i) precursors and the corresponding gold(i)–silver(i) heteronuclear derivatives, we have carried out single point DFT and TD-DFT calculations on model systems of complexes **2** and **4**. In the case of model **2**, it consists of the $[\text{Au}_2\{4\text{-C}_6\text{F}_4(4\text{-C}_6\text{BrF}_4)\}_2(\mu\text{-dppb})]$ structure obtained through X ray diffraction studies, whereas in the case of model **4** we have built up a model system using the X-ray diffraction results that is based on the dinuclear gold(i) moiety of model **2** with two dinuclear $[\text{Ag}_2(\text{CF}_3\text{CO}_2)_2]$ units, each one interacting with one gold(i) centre. We have also made an analysis of the electron density from the total SCF density mapped with electrostatic potential (ESPs) on these models in order to check which are the donor and the electron-acceptor parts of the molecule. Finally, the use of TD-DFT has allowed us to estimate the energy of the first triplet excitation that could be related to the phosphorescent emissions observed experimentally for both compounds.

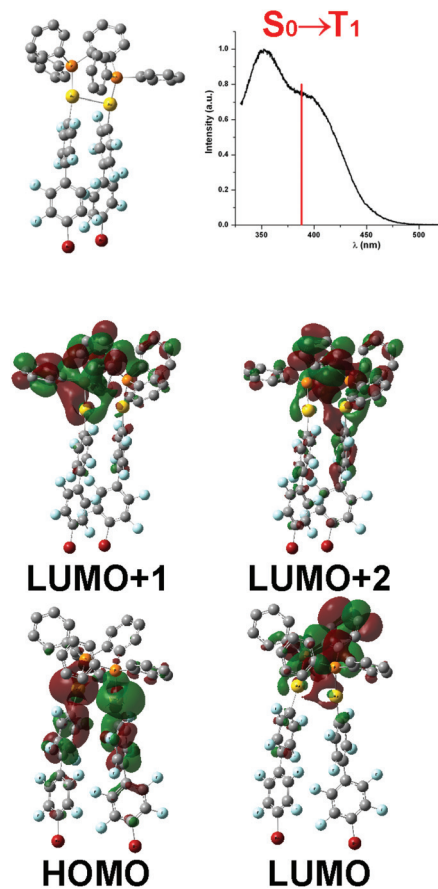


Fig. 7 Theoretical excitation energy (red line) compared to the excitation spectrum for complex **2** (up). Frontier molecular orbitals involved in the lowest triplet excitation for model $[\text{Au}_2(\text{C}_6\text{F}_4\text{-C}_6\text{F}_4\text{Br}_2)(\text{dppb})]$ representing complex **2** (bottom).

First, the nature of the frontier orbitals has been analysed from the results obtained in single-point DFT-B3LYP calculations (see Fig. 7 and 8). For the dinuclear gold(i) model $[\text{Au}_2\{4\text{-C}_6\text{F}_4(4\text{-C}_6\text{BrF}_4)\}_2(\mu\text{-dppb})]$ (**2**), the highest occupied molecular orbital HOMO is mostly located at the metal centres showing a $5d_{z^2}\sigma^*$ antibonding character (51% of contribution obtained from the population analysis), with some contribution from the perhalophenyl ligands (38%) and the diphosphine (11%). The population analysis of other highly occupied molecular orbitals (HOMO – 1 to HOMO – 5) shows a main contribution from the perhalophenyl ligands. By contrast, the lowest unoccupied molecular orbital LUMO is mainly centered at the phosphine ligand (89%) with a smaller contribution from the gold(i) centres (7%). A similar assignment of the LUMO orbital was recently proposed for dinuclear diphosphine gold(i) thiolate complexes.¹⁷ Other unoccupied molecular orbitals such as LUMO + 1 to LUMO + 3 are also mainly located at the phosphine ligand, although some small contributions from perhalophenyl groups and gold centres are also noticeable (see population analysis in Table 6).

In the case of model $[\text{Au}_2\text{Ag}_4\{4\text{-C}_6\text{F}_4(4\text{-C}_6\text{BrF}_4)\}_2(\text{CF}_3\text{CO}_2)_4(\mu\text{-dppb})]$, representing complex **4**, the character of the frontier orbitals shows significant differences with respect to that of

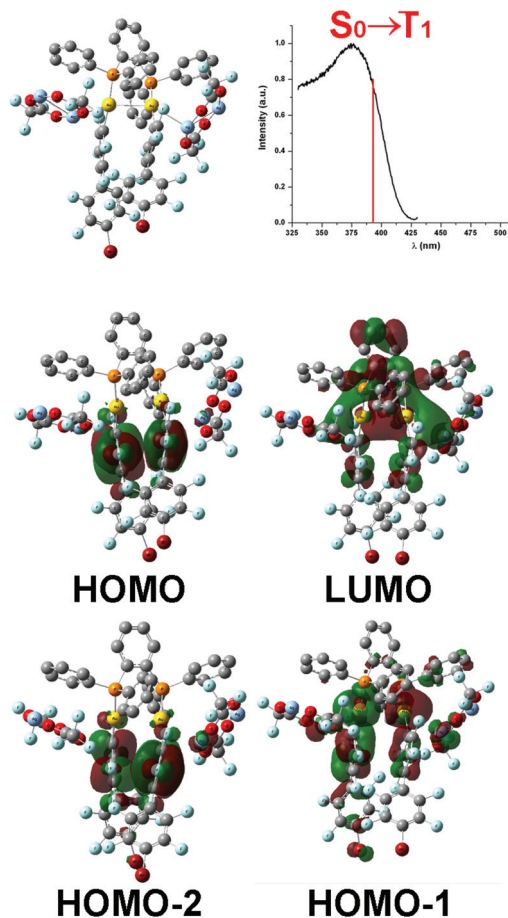


Fig. 8 Theoretical excitation energy (red line) compared to the excitation spectrum for complex **4** (up). Frontier molecular orbitals involved in the lowest triplet excitation for model $[\text{Au}_2\text{Ag}_4(\text{C}_6\text{F}_4\text{-C}_6\text{BrF}_4)_2(\text{CF}_3\text{CO}_2)_4(\text{dppb})]$ representing complex **4** (bottom).

Table 6 Population analysis showing the contribution of the different molecular parts for $[\text{Au}_2\{4\text{-C}_6\text{F}_4(4\text{-C}_6\text{BrF}_4)\}_2(\mu\text{-dppb})]$

Model (orbital)	%Au	%4-C ₆ F ₄ (4-C ₆ BrF ₄)	%dppb
(LUMO + 3)	9	23	68
(LUMO + 2)	10	12	78
(LUMO + 1)	10	5	85
(LUMO)	7	4	89
(HOMO)	51	38	11

model **2**. Thus, the HOMO orbital is mostly located (97%) at the bis(perhalophenyl) ligands bonded to gold(i), while the occupied orbital showing a $5d_z2\sigma^*$ antibonding character in the Au(i) metal centres (38%), with some contribution of the bis(perhalophenyl) ligands (32%), is now the HOMO - 1 orbital. Again, HOMO - 2 is placed at the bis(perhalophenyl) ligands. Another interesting difference is found for the character of the LUMO orbital, in which a larger metal-character is developed (23% at Au and 10% at Ag) if compared to model **2**, although the diphosphine is still the largest contribution to this orbital (48%) (see Fig. 8 and Table 7).

Table 7 Population analysis showing the contribution of the different molecular parts for $[\text{Au}_2\text{Ag}_4(4\text{-C}_6\text{F}_4(4\text{-C}_6\text{BrF}_4))_2(\text{CF}_3\text{CO}_2)_4(\mu\text{-dppb})]$

Model (orbital)	%Au	%Ag	%4-C ₆ F ₄ ⁻ (4-C ₆ BrF ₄)	%dppb	%CF ₃ CO ₂
(LUMO)	23	10	16	48	3
(HOMO)	2	0	97	0	1
(HOMO - 1)	38	14	32	12	4
(HOMO - 2)	1	2	95	1	1

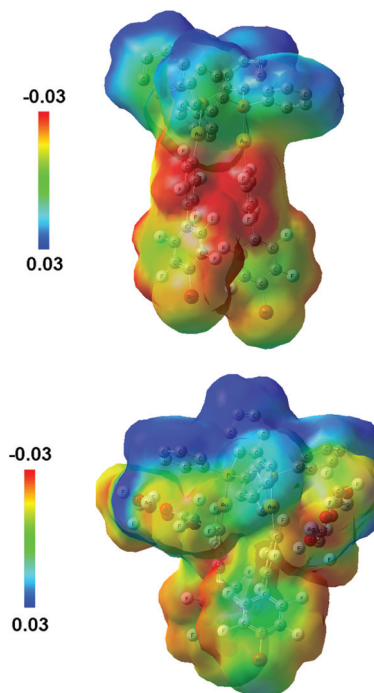


Fig. 9 Electron densities from the total SCF density mapped with electrostatic potentials (ESPs) for models of complexes **2** (up) and **4** (bottom).

In Fig. 9 we show the electron densities from the total SCF density mapped with electrostatic potentials (ESPs) for models **2** and **4**. In the case of model **2**, we observe that most of the electron density is located at the bis(perhalophenyl) groups and, to a less extent, at gold centres. It is worth mentioning that the electron-deficient part of the molecule is the phosphine ligand, what, together with the observed experimental results and the molecular orbital analysis, would suggest that the luminescence observed for this complex would arise from a mixed triplet ligand to ligand transition between the bis(perhalophenyl) ligand and the diphosphine ($^3\text{LLCT}$) and a metal (gold centres) to ligand (diphosphine) charge transfer transition ($^3\text{MLCT}$). In the case of model **4**, the colour contrast is not very clear but it seems that the electron-rich part of the molecule is mainly the anionic bis(perhalophenyl) ligands and, to a lesser extent, the gold(i) centres, whereas the diphosphine ligand and the silver centres are the electron-deficient part of the molecule. Again, this result would be in agreement with the experimental observations and the molecular orbital structure, which suggests that the emission in these

heteronuclear compounds would arise from a ligand to ligand charge transfer transition from the perhalophenyl groups to the diphosphine, although a small contribution from a transition among the metals could not be ruled out.

As we have commented above, complexes **2** and **4** display phosphorescent emissions at different energies. The use of the TD-DFT approach allows us to estimate the energy and molecular orbitals involved in the lowest triplet electronic excitation, which can be related to the observed emissions. The calculated triplet excitation energy for model **2** is 388 nm and it is comparable with the experimental excitation spectrum of complex **2** in solid state at room temperature (see Fig. 7). This triplet excitation arises from the occupied HOMO and arrives mainly to LUMO with some contributions from LUMO + 1 to LUMO + 3. Taking into account the above mentioned character for these orbitals, we can confirm the experimental and the theoretically predicted phosphorescent emission for complex **2**, based on the MO calculations and the electrostatic potentials as an admixture of a ³LLCT and a ³MLCT transition.

A similar TD-DFT analysis has been carried out for model system [Au₂Ag₄{4-C₆F₄(4-C₆BrF₄)₂}(CF₃CO₂)₄(μ-dppb)] representing complex **4**. The theoretically predicted triplet excitation energy of 393 nm fits fairly well with the experimental excitation maximum at 375 nm (see Fig. 8). In this case, the molecular orbitals involved in this electronic transition are the occupied HOMO to HOMO – 2 and the empty LUMO. This MO's combination would indicate that the experimentally observed phosphorescence would arise from a ³LLCT transition, involving MOs located at the bis(perhalophenyl) units as the starting orbitals and arriving to an orbital placed mainly at the diphosphine, although a contribution from the metals, both in the starting and the arriving orbitals, could not be neglected.

Conclusions

The use of different diphosphines, such as dppm or dppb, leads to the synthesis of a new class of bisaryldiphosphinegold(i) orange emitters. The addition of silver trifluoroacetate to the complexes [(Au{4-C₆F₄(4-C₆BrF₄)₂}(μ-L-L)] (L-L = dppm (**1**), dppb (**2**)) generates a very large shift of their emission maxima to the blue region.

Experimental results and DFT and TD-DFT calculations on the model system of **2** reveal an admixture of a ³LLCT and a ³MLCT transition as the origin for its phosphorescent behaviour, whereas on the model system of complex **4** phosphorescence would mainly arise from a ³LLCT transition.

Experimental

General

Silver trifluoroacetate, bis(diphenylphosphino)methane and 1,2-bis(diphenylphosphino)benzene are commercially available and were purchased from Aldrich.

Instrumentation

Infrared spectra were recorded in the 4000–200 cm⁻¹ range on a Nicolet Nexus FT-IR using Nujol mulls between polyethylene sheets. C, H analyses were carried out with a Perkin-Elmer 240C microanalyzer. Mass spectra were recorded on a Bruker Microflex MALDI-TOF, using dithranol (DIT) as a matrix. ¹H, ¹⁹F and ³¹P{¹H} NMR spectra were recorded on a Bruker ARX 300 in CDCl₃ solutions. Chemical shifts are quoted relative to SiMe₄ (¹H, external), CFCl₃ (¹⁹F, external) and H₃PO₄ (85%) (³¹P{¹H}, external). Luminescence spectra were recorded for solid samples with a Horiba Jobin Yvon Fluorolog 3 steady-state fluorescence spectrometer. This spectrometer was modified to allow for measurements of emission decay times. As excitation source a pulsed diode laser (PicoQuant GmbH Model LDH-P-C-375) with the excitation wavelength λ_{exc} = 372 nm and a pulse width of 100 ps was used. The emission was detected with a photomultiplier attached to a FAST ComTec multichannel scaler PCI card with a time resolution of 250 ps. Photoluminescence (PL) quantum yields were determined using a Hamamatsu system for absolute PL quantum yield measurements (type C9920-02) equipped with an integrating sphere with the Spectralon® inner surface coating.

Synthesis

Synthesis of [Au₂{4-C₆F₄(4-C₆BrF₄)₂}{μ-PPh₂CH₂PPh₂}] (1**) and [Au₂{4-C₆F₄(4-C₆BrF₄)₂}{μ-1,2-(C₆H₄)(PPh₂)₂}] (**2**).** To a solution of [Au{4-C₆F₄(4-C₆BrF₄)₂}(tbt)]¹¹ (0.227 mmol, 150.0 mg) in dichloromethane was added PPh₂CH₂PPh₂ (0.113 mmol, 44.0 mg) or 1,2-C₆H₄(PPh₂)₂ (0.113 mmol, 51.0 mg). After 1 h of stirring, the solution was concentrated under vacuum. Finally, the addition of *n*-hexane (5 mL) led to the precipitation of products **1** or **2** as white solids.

(**1**) Yield: 90%. Elemental analysis (%) calcd for **1** (C₄₉H₂₂Au₂Br₂F₁₆P₂): C 38.46, H 1.45. Found: C 39.04, H 1.48. ¹H NMR (300 MHz, CDCl₃, ppm): δ 7.80–7.28 (20H, C₆H₅) and 3.65 (t, 2H, CH₂, ²J_{(H-P)} = 9.2 Hz). ¹⁹F NMR (283 MHz, CDCl₃, ppm): δ -116.5 (m, 4F, F₁), -133.9 (m, 4F, F₂), -137.1 (m, 4F, F₃), -140.5 (m, 4F, F₄). ³¹P{¹H} NMR (121 MHz, CDCl₃, ppm): δ 32.3 (s). MALDI-TOF(-) *m/z* (%): 949 [Au{4-C₆F₄(4-C₆BrF₄)₂}]⁻ (100). FT-IR (Nujol): ν(4-C₆F₄(4-C₆BrF₄)) at 1629, 1597, 1571, 1097 and 858 cm⁻¹, ν(CH₂(PPh₂)₂) at 524, 509, 479 and 461 cm⁻¹.}

(**2**) Yield: 95%. Elemental analysis (%) calcd for **2** (C₅₄H₂₄Au₂Br₂F₁₆P₂): C 40.73, H 1.52. Found: C 40.85, H 1.50. ¹H NMR (300 MHz, CDCl₃, ppm): δ 7.62–7.26 (m, 24H). ¹⁹F NMR (283 MHz, CDCl₃, ppm): δ -114.7 (m, 4F, F₁), -133.5 (m, 4F, F₂), -137.2 (m, 4F, F₃), -141.0 (m, 4F, F₄). ³¹P{¹H} NMR (121 MHz, CDCl₃, ppm): δ 34.1 (s). MALDI-TOF(-) *m/z* (%): 949 [Au{4-C₆F₄(4-C₆BrF₄)₂}]⁻ (100). FT-IR (Nujol): ν(4-C₆F₄(4-C₆BrF₄)) at 1630, 1598, 1570, 1096 and 854 cm⁻¹, ν(1,2-C₆H₄(PPh₂)₂) at 548, 536, 516 and 501 cm⁻¹.

Synthesis of [Ag₂Au₂{4-C₆F₄(4-C₆BrF₄)₂}(CF₃CO₂)₂}{μ-PPh₂CH₂PPh₂}]_n (3**) and [Ag₂Au₂{4-C₆F₄(4-C₆BrF₄)₂}(CF₃CO₂)₂}{μ-1,2-C₆H₄(PPh₂)₂}]_n (**4**).** To a solution of [Au₂{4-C₆F₄(4-C₆BrF₄)₂}{μ-PPh₂CH₂PPh₂}] (**1**) (0.068 mmol, 105.0 mg) or

[Au₂{4-C₆F₄(4-C₆BrF₄)₂}{μ-1,2-(C₆H₄)(PPh₂)₂}] (2) (0.068 mmol, 108.0 mg) in dichloromethane (20 mL) was added AgCF₃CO₂ (0.136 mmol, 30.0 mg). After 1 h of stirring, the solution was concentrated under vacuum. Finally, the addition of *n*-hexane (5 mL) led to the precipitation of products 3 or 4 as pale yellow solids.

(3) Yield: 65%. Elemental analysis (%) calcd for 3 (C₅₃H₂₂Au₂Ag₂Br₂F₂₂O₄P₂): C 32.32, H 1.12. Found: C 32.40, H 1.15. ¹H NMR (300 MHz, CDCl₃, ppm): δ 7.79–7.28 (20H, C₆H₅) and 3.80 (t, 2H, CH₂, ²J_{(H-P)} = 11.0 Hz). ¹⁹F NMR (283 MHz, CDCl₃, ppm): δ -73.1 (s, 3F, -CF₃), -115.6 (m, 4F, F₁), -133.7 (m, 4F, F₂), -137.0 (m, 4F, F₃), -140.0 (m, 4F, F₄). ³¹P{¹H} NMR (121 MHz, CDCl₃, ppm): δ 32.4 (s). MALDI-TOF(+) *m/z* (%): 1065 [AgAu{4-C₆F₄(4-C₆BrF₄)}{μ-PPh₂CH₂PPh₂}]⁺ (50), 1639 [AgAu₂{4-C₆F₄(4-C₆BrF₄)₂}{μ-PPh₂CH₂PPh₂}]⁺ (25). FT-IR (Nujol): ν(4-C₆F₄(4-C₆BrF₄)) at 1571, 1102 and 856 cm⁻¹, ν(CF₃CO₂) at 1648 and 1174 cm⁻¹, ν(CH₂(PPh₂)₂) at 524, 508, 479 and 459 cm⁻¹.}

(4) Yield: 65%. Elemental analysis (%) calcd for 4 (C₅₈H₂₄Au₂Ag₂Br₂F₂₂O₄P₂): C 34.23, H 1.18. Found: C 34.45, H 1.19. ¹H NMR (300 MHz, CDCl₃, ppm): δ 7.61–7.28 (24H, C₆H₅). ¹⁹F NMR (283 MHz, CDCl₃, ppm): δ -73.1 (s, 3F, -CF₃), -114.2 (m, 4F, F₁), -133.4 (m, 4F, F₂), -137.2 (m, 4F, F₃), -141.0 (m, 4F, F₄). ³¹P{¹H} NMR (121 MHz, CDCl₃, ppm): δ 33.9 (s). MALDI-TOF(-) *m/z* (%): 333 [Ag(CF₃CO₂)₂]⁻ (100), 555 [Ag₂(CF₃CO₂)₃]⁻ (25). FT-IR (Nujol): ν(4-C₆F₄(4-C₆BrF₄)) at 1098 and 856 cm⁻¹, ν(CF₃CO₂) at 1645 and 1197 cm⁻¹, ν(CH₂(PPh₂)₂) at 547, 534, 518 and 501 cm⁻¹.

Crystallography

Crystals were mounted in inert oil on glass fibers and transferred to the cold gas stream of a Nonius Kappa CCD diffractometer equipped with an Oxford Instruments low-temperature attachment. Data were collected using monochromated Mo Kα radiation (λ = 0.71073 Å). Scan type ω and φ. Absorption corrections: semiempirical (based on multiple scans). The structures were solved by direct methods and refined on F² using the program SHELXL-97.¹⁸ All non-hydrogen atoms were refined anisotropically. Hydrogen atoms were included using a riding model. Further details of the data collection and refinement are given in Table 1. Selected bond lengths and angles are collected in Tables 2–4 and crystal structures of complexes 2–4 in Fig. 2–4. In spite of absorption corrections have been carried out, the low quality of the crystals and the high absorption coefficients have given rise to the presence of slightly high residual density peaks. Similarly, due to the same reasons, the value of *S* parameter in complex 4 is slightly larger than usually. CCDC-891443–891445 contains the supplementary crystallographic data for this paper.

Computational details

The model systems used in the theoretical studies of [Au₂{4-C₆F₄(4-C₆BrF₄)₂}(μ-dppb)] and [Au₂Ag₄{4-C₆F₄(4-C₆BrF₄)₂}(CF₃CO₂)₄}(μ-dppb)] were taken from the X ray diffraction data for complexes 2 and 4. Keeping all distances, angles and dihedral angles frozen, single-point DFT or TD-DFT calculations

were performed. The B3LYP functional¹⁹ as implemented in GAUSSIAN09²⁰ was used. In all calculations, the Karlsruhe split-valence quality basis sets²¹ augmented with polarization functions²² were used (SVP). The Stuttgart effective core potentials of Andrae augmented with two f-type polarization functions were used for Au and Ag.²³ The population analysis has been carried out using the GaussSum 2.2 program.²⁴ We have also carried out an analysis of the electron densities from the total SCF density mapped with electrostatic potentials (ESPs) for model systems [Au₂{4-C₆F₄(4-C₆BrF₄)₂}(μ-dppb)] and [Au₂Ag₄{4-C₆F₄(4-C₆BrF₄)₂}(CF₃CO₂)₄}(μ-dppb)].

Acknowledgements

The German Federal Ministry of Education and Research (BMBF) and D.G.I.(MEC)/FEDER (project number CTQ2010-20500-C02-02) are acknowledged for the funding of our research. T. L. thanks MICINN for a grant. J. M. L-de-L and H. Y. acknowledge the receipt of an MICINN-DAAD joint project (HD2008-0022). The authors thank to the Centro de Supercomputación de Galicia (CESGA) for computational resources.

Notes and references

- (a) H. Schmidbauer, in *Gold: Progress in Chemistry, Biochemistry and Technology*, John Wiley & Sons, New York, 1999; (b) H. Schmidbauer, *Nature*, 2001, **413**, 31; (c) H. Schmidbauer, *Gold Bull.*, 1990, **23**, 11.
- (a) P. Pykkö, *Chem. Rev.*, 1997, **97**, 597; (b) P. Pykkö, *Angew. Chem., Int. Ed.*, 2004, **43**, 4412; (c) P. Pykkö, *Inorg. Chim. Acta*, 2005, **358**, 4113; (d) P. Pykkö, *Chem. Soc. Rev.*, 2008, **37**, 1967.
- (a) J. M. Forward, J. P. Fackler Jr. and Z. Assefa, in *Optoelectronic Properties of Inorganic Compounds*, ed. D. M. Roundhill and J. P. Fackler Jr., Plenum, New York, 1999, pp. 195–226; (b) J. M. López-de-Luzuriaga, in *Modern Supramolecular Gold Chemistry*, ed. A. Laguna, Wiley-VCH, Weinheim, 2008, p. 347.
- (a) E. J. Fernández, A. Laguna, J. M. López-de-Luzuriaga and M. Monge, *Spanish Patent*, P200001391, 2003; (b) E. J. Fernández, J. M. López-de-Luzuriaga, M. Monge, M. E. Olmos, J. Pérez, A. Laguna, A. A. Mohammed and J. P. Fackler Jr., *J. Am. Chem. Soc.*, 2003, **125**, 2022; (c) E. J. Fernández, J. M. López-de-Luzuriaga, M. Monge, M. Montiel, M. E. Olmos, J. Pérez, A. Laguna, F. Mendizábal, A. A. Mohamed and J. P. Fackler Jr., *Inorg. Chem.*, 2004, **43**, 3573; (d) E. J. Fernández, J. M. López-de-Luzuriaga, M. Monge, M. E. Olmos, R. C. Puelles, A. Laguna, A. A. Mohamed and J. P. Fackler Jr., *Inorg. Chem.*, 2008, **47**, 8069.
- (a) A. Vogler and H. Kunkely, *Coord. Chem. Rev.*, 2001, **489**, 219; (b) E. J. Fernández, A. Laguna and M. E. Olmos, *Adv. Organomet. Chem.*, 2005, **52**, 77.

- 6 (a) E. J. Fernández, A. Laguna, J. M. López-de-Luzuriaga, M. Monge, M. Montiel and M. E. Olmos, *Inorg. Chem.*, 2007, **46**, 2953; (b) E. J. Fernández, A. Laguna, J. M. López-de-Luzuriaga, M. Montiel, M. E. Olmos and J. Pérez, *Organometallics*, 2005, **24**, 1631; (c) E. J. Fernández, A. Laguna, J. M. López de Luzuriaga, F. Mendizabal, M. Monge, M. E. Olmos and J. Pérez, *Chem.-Eur. J.*, 2003, **9**, 456; (d) E. J. Fernández, J. M. López-de-Luzuriaga, M. Monge, M. E. Olmos, J. Pérez and A. Laguna, *J. Am. Chem. Soc.*, 2002, **124**, 5942; (e) E. J. Fernández, P. G. Jones, A. Laguna, J. M. López-de-Luzuriaga, M. Monge, J. Pérez and M. E. Olmos, *Inorg. Chem.*, 2002, **41**, 1056; (f) O. Crespo, E. J. Fernández, P. G. Jones, A. Laguna, J. M. López-de-Luzuriaga, A. Mendía, M. Monge and M. E. Olmos, *Chem. Commun.*, 1998, 2233; (g) P. G. Jones and C. Thöne, *Acta Crystallogr., Sect. C: Cryst. Struct. Commun.*, 1992, **48**, 1312; (h) M. A. Bennet, D. C. R. Hockless, A. D. Rae, L. L. Welling and A. C. Willis, *Organometallics*, 2001, **20**, 79; (i) M. Bardají, P. G. Jones, A. Laguna, M. D. Villacampa and N. Valverde, *Dalton Trans.*, 2003, 4529; (j) R. Usón, A. Laguna, M. Laguna, I. Colera and E. De Jesús, *J. Organomet. Chem.*, 1984, **263**, 121.
- 7 (a) E. J. Fernández, A. Laguna, J. M. López-de-Luzuriaga, M. Montiel, M. E. Olmos, J. Pérez and R. C. Puelles, *Organometallics*, 2006, **25**, 4307; (b) E. J. Fernández, A. Laguna, J. M. López-de-Luzuriaga, M. Monge, M. Montiel, M. E. Olmos, J. Pérez, R. C. Puelles and J. C. Sáenz, *J. Chem. Soc., Dalton Trans.*, 2005, 1162.
- 8 E. J. Fernández, P. G. Jones, A. Laguna, J. M. López-de-Luzuriaga, M. Monge, M. E. Olmos and R. C. Puelles, *Organometallics*, 2007, **26**, 5931.
- 9 E. J. Fernández, C. Hardacre, A. Laguna, M. C. Lagunas, J. M. López-de-Luzuriaga, M. Monge, M. Montiel, M. E. Olmos, R. C. Puelles and E. Sánchez-Forcada, *Chem.-Eur. J.*, 2009, **16**, 6222.
- 10 R. Usón, A. Laguna, M. Laguna, I. Colera and E. De Jesús, *J. Organomet. Chem.*, 1984, **263**, 121.
- 11 (a) X. Honk, K. K. Cheung, C. X. Guo and C.-M. Che, *J. Chem. Soc., Dalton Trans.*, 1994, 1867; (b) M. Bardají, P. G. Jones, A. Laguna, A. Moracho and A. K. Fischer, *J. Organomet. Chem.*, 2002, **648**, 1.
- 12 T. Pilati, P. Metrangolo and G. Resnati, *Acta Crystallogr.*, 2001, **57**, 113.
- 13 A. Pintado-Alba, H. de la Riva, M. Niewhuyzen, D. Bautista, P. R. Raithby, H. A. Sparkes, S. J. Teat, J. M. López-de-Luzuriaga and M. C. Lagunas, *Dalton Trans.*, 2004, 3459.
- 14 (a) H. Yersin, A. F. Rausch, R. Czerwieniec, T. Hofbeck and T. Fischer, *Coord. Chem. Rev.*, 2011, **255**, 2622; (b) T. Hofbeck and H. Yersin, *Inorg. Chem.*, 2010, **49**, 9290; (c) D. N. Kozhevnikov, V. N. Kozhevnikov, M. M. Ustinova, A. Santoro, D. W. Bruce, B. Koenig, R. Czerwieniec, T. Fischer, M. Zabel and H. Yersin, *Inorg. Chem.*, 2009, **48**, 4179; (d) S. Jamali, R. Czerwieniec, R. Kia, Z. Jamshidi and M. Zabel, *Dalton Trans.*, 2011, **40**, 9123; (e) R. Czerwieniec, T. Hofbeck, O. Crespo, A. Laguna, M. C. Gimeno and H. Yersin, *Inorg. Chem.*, 2010, **49**, 3764; (f) V. N. Kozhevnikov, M. C. Durrant and J. A. G. Williams, *Inorg. Chem.*, 2011, **50**, 6304; (g) A. F. Rausch, L. Murphy, J. A. G. Williams and H. Yersin, *Inorg. Chem.*, 2012, **51**, 312; (h) M. Panigati, M. Mauro, D. Donghi, P. Mercandelli, P. Mussini, L. De Cola and G. D'Alfonso, *Coord. Chem. Rev.*, 2012, **256**, 1621; (i) L. Murphy, P. Brulatti, V. Fattori, M. Cocchi and J. A. G. Williams, *Chem. Commun.*, 2012, **48**, 5817; (j) C.-W. Hsu, C.-C. Lin, M.-W. Chung, G.-H. Lee, P. T. Chou, C.-H. Chang and P. Y. Chen, *J. Am. Chem. Soc.*, 2011, **133**, 12085.
- 15 A. F. Rausch, H. H. H. Homeier and H. Yersin, *Top. Curr. Chem.*, 2010, **29**, 193.
- 16 A. Kapturkiewicz and G. Angulo, *Dalton Trans.*, 2003, 3907.
- 17 P. J. Costa and M. J. Calhorda, *Inorg. Chim. Acta*, 2006, **359**, 3617.
- 18 G. M. Sheldrick, *SHELXL-97, Program for Crystal Structure Refinement*, University of Göttingen, Germany, 1997.
- 19 (a) A. D. Becke, *J. Chem. Phys.*, 1992, **96**, 215; (b) A. D. Becke, *J. Chem. Phys.*, 1993, **98**, 5648; (c) C. Lee, W. Yang and R. G. Parr, *Phys. Rev. Lett.*, 1998, **37**, 785.
- 20 M. J. Frisch, G. W. Trucks, H. B. Schlegel, G. E. Scuseria, M. A. Robb, J. R. Cheeseman, G. Scalmani, V. Barone, B. Mennucci, G. A. Petersson, H. Nakatsuji, M. Caricato, X. Li, H. P. Hratchian, A. F. Izmaylov, J. Bloino, G. Zheng, J. L. Sonnenberg, M. Hada, M. Ehara, K. Toyota, R. Fukuda, J. Hasegawa, M. Ishida, T. Nakajima, Y. Honda, O. Kitao, H. Nakai, T. Vreven, J. A. Montgomery Jr., J. E. Peralta, F. Ogliaro, M. Bearpark, J. J. Heyd, E. Brothers, K. N. Kudin, V. N. Staroverov, R. Kobayashi, J. Normand, K. Raghavachari, A. Rendell, J. C. Burant, S. S. Iyengar, J. Tomasi, M. Cossi, N. Rega, N. J. Millam, M. Klene, J. E. Knox, J. B. Cross, V. Bakken, C. Adamo, J. Jaramillo, R. Gomperts, R. E. Stratmann, O. Yazyev, A. J. Austin, R. Cammi, C. Pomelli, J. W. Ochterski, R. L. Martin, K. Morokuma, V. G. Zakrzewski, G. A. Voth, P. Salvador, J. J. Dannenberg, S. Dapprich, A. D. Daniels, Ö. Farkas, J. B. Foresman, J. V. Ortiz, J. Cioslowski, D. J. Fox, *GAUSSIAN 09 (Revision A.1)*, Gaussian, Inc., Wallingford CT, 2009.
- 21 A. Schäfer, H. Horn and R. Ahlrichs, *J. Chem. Phys.*, 1992, **97**, 2571.
- 22 T. H. Dunning Jr., *J. Chem. Phys.*, 1994, **100**, 5829.
- 23 D. Andrae, U. Haeussermann, M. Dolg, H. Stoll and H. Preuss, *Theor. Chim. Acta*, 1990, **77**, 123.
- 24 N. M. Boyle, A. L. Tenderholt and K. M. Langner, *J. Comput. Chem.*, 2008, **29**, 839.